



Effects of dielectric barrier discharge plasma on the catalytic activity of Pt/CeO₂ catalysts



Bangfen Wang^a, Bingxu Chen^a, Yuhai Sun^a, Hailin Xiao^a, Xiaoxin Xu^a, Mingli Fu^{a,b,c}, Junliang Wu^{a,b,c}, Limin Chen^{a,b,c}, Daiqi Ye^{a,b,c,*}

^a School of Environment and Energy, South China University of Technology, Guangzhou 510006, China

^b National Engineering Laboratory for VOCs Pollution Control Technology and Equipment, Guangzhou 510006, China

^c Guangdong Provincial Key Laboratory of Atmospheric Environment and Pollution Control, Guangzhou 510006, China

ARTICLE INFO

Keywords:

Dielectric barrier discharge
Pt/CeO₂ catalysts
Plasma effect
Toluene oxidation

ABSTRACT

CeO₂ nanorod was synthesized by a hydrothermal method and impregnated with Pt to synthesize Pt/CeO₂ catalysts, which were modified by dielectric barrier discharge plasma. The modified CeO₂ and Pt/CeO₂ were characterized by XRD, STEM, N₂ adsorption/desorption, CO pulse chemisorption, XPS, H₂-TPR, O₂-TPD and UV-Raman spectroscopy techniques. After the plasma treatment, the T₉₀ value of (Pt/CeO₂)-P catalyst decreased from 287 °C to 208 °C for toluene oxidation. This significantly changed activity of catalyst indicated that plasma has greatly impacted its performance. More and larger notches on surface and broken fragments were found from STEM analysis. In addition, smaller Pt particle size and higher dispersion of nanoparticles was found on (Pt/CeO₂)-P, which was characterized by CO pulse chemisorption and TEM analysis. In addition, Pt/(CeO₂-P) and (Pt/CeO₂)-P possessed higher concentration of oxygen vacancies and Ce³⁺, which was observed by UV-Raman spectroscopy and XPS. Moreover, according to TPR results, the interaction between Pt and CeO₂ was obviously strengthened, which led to a lower reduction temperature after plasma treatment. After plasma treatment, the (Pt/CeO₂)-P presented the highest activity due to it possessing the highest TOF_{Pt} and TOF_{ov} values of $9.88 \times 10^{-4} \text{ s}^{-1}$ and $9.49 \times 10^{-5} \text{ s}^{-1}$, respectively, and lower activation energies of 63.8 kJ mol⁻¹. Furthermore, the toluene conversion of (Pt/CeO₂)-P without significantly decreasing for working at least 50 h and under 9.6 vol% water vapor.

1. Introduction

Non-thermal plasma (NTP) technology is a very useful and widely used technology for environmental pollution control and energy reproduction. It is commonly applied in the abatement of volatile organic compounds (VOCs) [1,2], the production of hydrogen and fuel reforming [3,4], and is also used for modifying or manufacturing of catalyst, such as the synthesis of nanomaterials via a plasma treatment under ambient conditions [5,6], and pretreatment of nanocatalysts by H₂, Ar and O₂ plasma under low temperature to enhance and increase catalytic activity and stability [7–9]. The main effects of plasma on catalytic oxidation of catalysts are to change the structural properties of the catalyst (morphological, surface area, dispersion and particle size) and generate to more active species exposed on the catalyst surface, and increasing the activity and stability of catalyst under atmospheric or ordinary pressure (500 Torr) [10–12]. Therefore, plasma treatment is an effective method of modifying or manufacturing of catalyst. More

active sites and a large surface area could be generated for catalysts exposed to a plasma discharge zone under atmospheric pressure [13]. Rahmani et al. [14] utilized Ar glow discharge plasma on the synthesized Pt/CeO₂-Al₂O₃ nanocatalysts to enhance the toluene-oxidized activity under atmospheric pressure. Results of the elemental analysis showed a high dispersion of elemental Pt and a good distribution of the desirable elements in the catalyst structure of catalyst. Chen et al. [15] determined that Au/ZSM-5 catalyst showed the best oxidative activity when pretreated by a non-thermal O₂ plasma method compared to conventional calcinations and reduction under ordinary pressure. The high oxidation was explained as being due to a smaller size particle and more uniform dispersion of Au particles on the ZSM-5 surface. Lu et al. [16] used MnO_x as an active component loaded onto SBA-15 and exposed to a non-thermal atmospheric plasma system, which resulted in the detection of the Mn₃O₄ species with larger oxidation capability after discharge. Hinokuma et al. [17] investigated the catalytic activity of Pd/CeO₂ prepared using arc-plasma under atmospheric pressure, and

* Corresponding author at: School of Environment and Energy, South China University of Technology, Guangzhou 510006, China.

E-mail address: cedqye@scut.edu.cn (D. Ye).

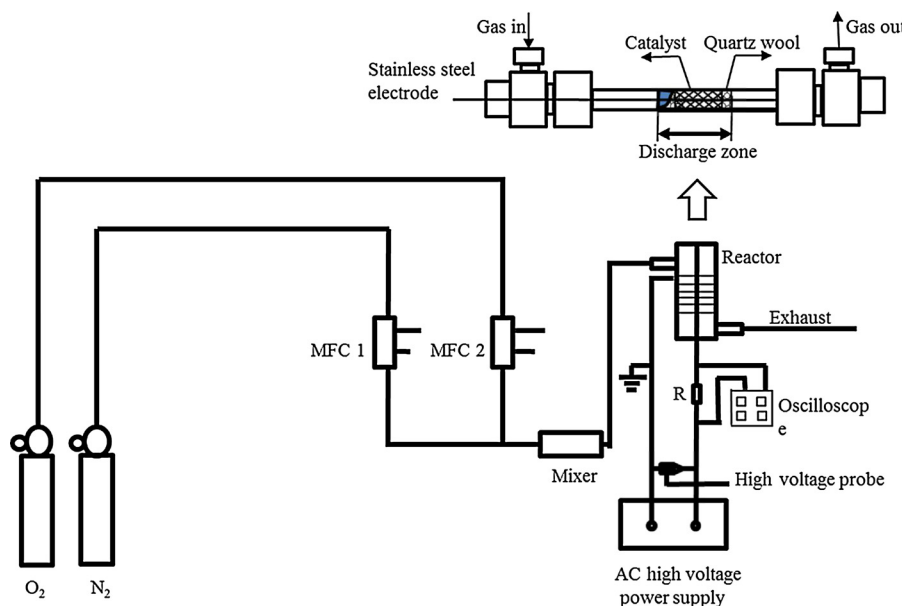


Fig. 1. Schematic of DBD system for plasma treatment of catalysts.

results showed that the as-prepared catalyst exhibited a higher catalytic activity ($\text{TOF} = 0.60$) than catalysts prepared via conventional wet-impregnation ($\text{TOF} = 0.12$). Thus, more research has focused on the particle size of active components modified by plasma. However, few studies for effect of air plasma on catalyst supports and strong interaction with active components, which play an important role in the catalytic oxidation process.

CeO_2 loaded with platinum (Pt/CeO_2) catalysts have been extensively applied for thermo-catalytic oxidation. CeO_2 exhibits an extensive reducibility and high oxygen storage capacity, and the activity of CeO_2 based on the ease of the reversible $\text{Ce}^{4+}/\text{Ce}^{3+}$ redox cycles. The activity of CeO_2 can be affected by many factors, such as crystal facets and textural properties, as well as by the concentration and distribution of oxygen vacancies [18–20]. Pt/CeO_2 was considered a promising catalyst to enhance the performance of catalytic materials [21]. The distribution and size of Pt particles are crucial to enhancing the activity performance of Pt/CeO_2 in catalytic processes [22]. Chen et al. [23] studied the size of Pt nanoparticles on $\text{Pt}/\text{ZSM-5}$ ranging from 1.3 to 2.3 nm, and found that Pt-1.9 catalyst had the highest activity for toluene oxidation due to its relatively higher Pt dispersion. Peng et al. [24] determined that Pt/CeO_2 -1.8 catalyst exhibited the best catalytic performance due to its high Pt dispersion and oxygen vacancies concentration of ceria. In addition, the metal-supporter interaction/synergy also played an important role in the catalytic oxidation [23,24]. According to the previous references on plasma effects on catalyst, various catalysts were pretreated by plasma and test results indicated that the activities were enhanced in terms of catalytic oxidation of VOCs [25–27]. Therefore, plasma would seem to be an effective means of solving the crucial issue of distribution of Pt nanoparticles on the CeO_2 surface. However, the effects of plasma on the support and active component of Pt/CeO_2 for catalytic oxidation of toluene are unclear. Hence, CeO_2 and Pt/CeO_2 are introduced as the objects of study in this paper, and some specific properties are proved by characterization and investigation of catalytic processes to better understand the effect of plasma on catalyst. As one of the classic VOCs, toluene is introduced as the probe to evaluate the catalytic activity of CeO_2 -based catalysts [28].

In this work, the Pt/CeO_2 used was produced by a simple impregnation method that was modified by air-plasma treatment upon loading after discharge and upon loading before discharge at room temperature and atmospheric pressure. The obtained catalysts were used for toluene

removal. XRD, STEM, N_2 adsorption/desorption, CO-pulse chemisorption, XPS, H_2 -TPR, O_2 -TPD and UV-Raman spectroscopy techniques were used to characterize and analyze the effects of plasma on catalyst. Additionally, the TOFs of Pt particles as well as oxygen vacancy and activation energies were studied for Pt/CeO_2 catalysts pretreated by DBD plasma. In addition, the stability and water resistance of Pt/CeO_2 and $(\text{Pt}/\text{CeO}_2)\text{-P}$ catalysts under conditions of toluene oxidation were tested.

2. Experimental

2.1. Catalyst preparation

2.1.1. Synthesis of CeO_2 nanorods

Pure CeO_2 was synthesized by a hydrothermal method. 5 mmol of cerous acetate ($(\text{CH}_3\text{COO})_3\text{Ce}\cdot\text{xH}_2\text{O}$, Aladdin) were dissolved in 20 ml of deionized water, 55 ml of 7 mol L^{-1} NaOH solution were added to form a translucent solution after stirring for 30 min, the mixed solution was then transferred to a 100 ml of Teflon-lined stainless-steel autoclave, which was then placed in temperature-programmed oven for 5 h at 130 °C, followed by cooling to room temperature. Finally, the precipitate was washed with deionized water and absolute alcohol several times to neutrality ($\text{pH} = 7$), and dried at 100 °C for 24 h. The obtained pure CeO_2 was divided into two parts. One part was treated by plasma and is referred to as $\text{CeO}_2\text{-P}$.

2.1.2. Preparation of Pt/CeO_2

A simple impregnation method was used to fabricate Pt/CeO_2 and $\text{Pt}/(\text{CeO}_2\text{-P})$. A certain amount of platinum nitrate-solution (99.99% grade, metal basis, Sigma-Aldrich) was added in solution with CeO_2 and $\text{CeO}_2\text{-P}$, and stirred well. After 24-h the impregnation procedure at room temperature, the catalysts were dried at 100 °C overnight. Finally, the powders were calcined at 400 °C for 5 h in dry air. The CeO_2 and $\text{CeO}_2\text{-P}$ loaded Pt were denoted Pt/CeO_2 and $\text{Pt}/(\text{CeO}_2\text{-P})$, respectively. Part of Pt/CeO_2 catalyst was modified by DBD plasma and denoted $(\text{Pt}/\text{CeO}_2)\text{-P}$.

2.1.3. Dielectric barrier discharge system

Plasma treatment of the catalyst was conducted on a custom DBD plasma system. The schematic and catalyst-packed DBD reactor are shown in Fig. 1. The catalyst modified apparatus consisted of a quartz

tube (ϕ 8 mm), stainless steel electrode (ϕ 1 mm) system and discharge zone 80 mm length. Catalyst was filled into the discharge zone of the reactor for the dry air plasma treatment. High-voltage with an AC frequency of 1.8 kHz was applied and the input power measured by an oscilloscope. The discharge condition was set for 30 min with 4.8 W of input power, a flow of 20% O₂ and 80% N₂, and a flow of 100 ml min⁻¹.

2.2. Catalyst characterization

The XRD (X-ray diffraction) patterns were recorded by diffractometer (D8 ADVANCE, Bruker, Germany) with Cu K α radiation (40 kV, 40 mA, scanning step of 0.02) to obtain the crystalline structure. The N₂ adsorption-desorption isotherms and pore distribution were measured on an ASAP 2020 system (Micromeritics, USA) in static measurement mode at 77 K, and the specific surface area was calculated using the Brunauer-Emmett-Teller (BET) model. The samples contained a certain wt% of Pt as determined by inductively coupled plasma atomic absorption spectroscopy (ICP-AAS).

STEM (Scanning transmission electron microscopy) images were obtained using a Zeiss Ultra device (Germany) at an accelerating voltage of 3 kV. The Pt content was determined from the inductively coupled plasma with an atomic absorption spectrometer (Z-2000, Hitachi Ltd., Japan). The average diameters of the platinum particle ($d_{1\text{Pt}}$) were estimated from the TEM images based on the Eq. (R1) below. The dispersion of Pt nanoparticles (NPs) over the catalyst ($D_{1\text{Pt}}$) was calculated according to Eq. (R2).

Static CO-pulse chemisorption was measured on a Micromeritics AutoChem II 2920 to calculate the metal dispersion of Pt on CeO₂. A 100 mg sample was placed in a U-shaped quartz tube. Samples were pre-reduced at 300 °C for 3 h in 10% H₂/Ar flow (30 ml min⁻¹) to convert metal oxide into a metallic state. After the subsequent temperature was cooled to 30 °C under Ar flow (30 ml min⁻¹), and then 10% CO/Ar pulse stream was periodically injected until the adsorption reached the saturation of the catalyst. Then, the dispersion ($D_{2\text{Pt}}$) and diameter ($d_{2\text{Pt}}$) of the Pt NPs were evaluated [Eqs. (R3) and (R4)] according to the consumption of CO.

Note that the Pt NPs assumed a spherical shape for all the following analyses reported in this paper.

$$d_{1\text{Pt}} \approx \frac{\sum_i n_i d_i}{\sum_i n_i} \quad (\text{R1})$$

$$D_{1\text{Pt}} = \frac{600M_{\text{Pt}}}{\rho_{\text{Pt}} d_{\text{Pt}} \alpha_{\text{Pt}} N_A} \quad (\text{R2})$$

$$d_{2\text{Pt}} = \frac{60X_{\text{Pt}}}{\rho_{\text{Pt}} S_{\text{Pt}}} \quad (\text{R3})$$

$$D_{2\text{Pt}} = \frac{10S_{\text{Pt}} M_{\text{Pt}}}{X_{\text{Pt}} \alpha_{\text{Pt}} N_A} \quad (\text{R4})$$

where n_i is the number of particles of diameter d_i (nm), M_{Pt} the molar weight of Pt (195.08 g mol⁻¹), ρ_{Pt} the density of Pt (21.45 g cm⁻³), α_{Pt} the cross-sectional area of Pt atoms (8.06×10^{-20} m² atom⁻¹), N_A Avogadro constant (6.019×10^{23} atom mol⁻¹), S_{Pt} the surface area of Pt relative to the sample obtained from CO pulse chemisorption (m² g⁻¹), and X_{Pt} the amount of Pt loaded (%). The stoichiometric ratio of CO and the Pt atom was set as 1:1.

XPS (X-ray photoelectron spectroscopy) analysis of catalyst was carried out using a Thermo ESCALAB 250 with Al K α ($h\nu = 1486.8$ eV) as the excitation source. The shifts of samples were corrected by setting the binding energy of the adventitious carbon (C 1s) to 284.6 eV. UV-Raman spectroscopy measurements of all Pt/CeO₂ samples were collected with a LabRAM HR Evolution laser Raman spectrometer (HYJ, France) equipped with a Kinmon He-Cd laser (325 nm) and a CCD

(charge-coupled-device) detector with spectral resolution of 1 cm⁻¹. The 325 nm laser-power excitation on the sample was kept at 8 mW.

Hydrogen temperature-programmed reduction (H₂-TPR) experiments were carried out on a chemisorption analyzer (Micromeritics AutoChem II 2920). 100 mg sample was weighed and first purge treated under a pure Ar flow (30 ml min⁻¹) at 300 °C for 30 min. It was then heated (10 °C min⁻¹) from room temperature to 600 °C in a flowing 10% H₂/Ar mixture (30 ml min⁻¹).

Oxygen temperature programmed desorption (O₂-TPD) experiments were carried out on the above-mentioned AutoChem II 2920. A 100 mg sample was weighed and reduced in a flowing 10% H₂/Ar mixture (30 ml min⁻¹) at 300 °C for 180 min. It was then cooled to 60 °C in He (30 ml min⁻¹) and stabilized by adsorbed 5% O₂/He (30 ml min⁻¹) for 60 min. Finally, it was heated (10 °C min⁻¹) from room temperature to 500 °C in a flow of He (30 ml min⁻¹).

Oxygen-pulse chemisorption measurements were conducted on the same chemisorption analyzer to quantify the amount of O₂ adsorbed on catalysts after reduction. A 100 mg sample was weighed and reduced in a flowing 10% H₂/Ar mixture (30 ml min⁻¹) at 300 °C for 180 min. The sample was cooled to 30 °C in He (30 ml min⁻¹), and after being stabilized, 5% O₂/He (30 ml min⁻¹) was pulsed multiple times onto the sample until saturation was reached. The consumption of O was accordingly calculated and defined as OSC_{Catal}, and the consumption of Pt was defined as OSC_{Pt}, the latter was calculated based on Eq. (R5) below and the stoichiometric ratio of O and the metal atom was set as 2:1. The quality of surface oxygen vacancy concentration was defined as OSC_{surf} and calculated by Eq. (R6). The data are shown in Table S1.

$$\text{OSC}_{\text{Pt}} = \frac{2D_{\text{Pt}} X_{\text{Pt}}}{M_{\text{Pt}}} 10^2 \quad (\text{R5})$$

$$\text{OSC}_{\text{Surf}} = \text{OSC}_{\text{Catal}} - \text{OSC}_{\text{Pt}} \quad (\text{R6})$$

2.3. Catalytic activity evaluation

The catalytic activities of the catalysts were evaluated by measuring the degree of thermo-catalytic oxidation in a reactor made of 50 cm quartz tubes with an 8 nm internal diameter and 10 nm external. The catalyst (120 mg, 40–60 mesh) was mixed with 600 mg of silicon (40–60 mesh) to heat the catalyst evenly. The total flow rate was 100 ml min⁻¹ (WHSV (weight hourly space velocity) at 50,000 ml g⁻¹ h⁻¹) with a 200 ppm concentration of toluene in 20% O₂/N₂. The reaction system was heated to a given temperature and then oxidized. After the reaction, the products were analyzed online using a gas chromatograph (GC-2014C, Shimadzu, Corp., Japan) equipped with a FID detector. Before the reaction, all the catalysts were reduced in 10% H₂/N₂ flow at 60 ml min⁻¹ at 300 °C for 3 h. The conversion of toluene oxidation to CO₂ (η , %) [Eq. (R7)] was carried out on the toluene oxidation. The values of TOF_{Pt} [Eq. (R8)] and TOF_{Ov} [Eq. (R9)] were calculated from the conversion of a certain amount of toluene per second over per atom of Pt at 150 °C. Activation energies (E_a) were calculated at lower than 10% toluene conversion and determined by the Arrhenius plot.

$$\eta = \frac{C_{\text{CO}_2}}{7C_0} \times 100\% \quad (\text{R7})$$

$$\text{TOF}_{\text{Pt}}(\text{s}^{-1}) = 100\eta F_{\text{tol}} \frac{M_{\text{Pt}}}{m_{\text{cat}} X_{\text{Pt}} D_{\text{Pt}}} \quad (\text{R8})$$

$$\text{TOF}_{\text{Ov}}(\text{s}^{-1}) = \eta F_{\text{tol}} \frac{1}{m_{\text{Cat}} \text{OSC}_{\text{Surf}}} \quad (\text{R9})$$

where C₀ is the inlet concentration of toluene (ppm), C_{CO₂} the outlet concentration of CO₂ (ppm), F_{tol} the toluene velocity (mol s⁻¹), and m_{cat} quantity of catalyst (g).

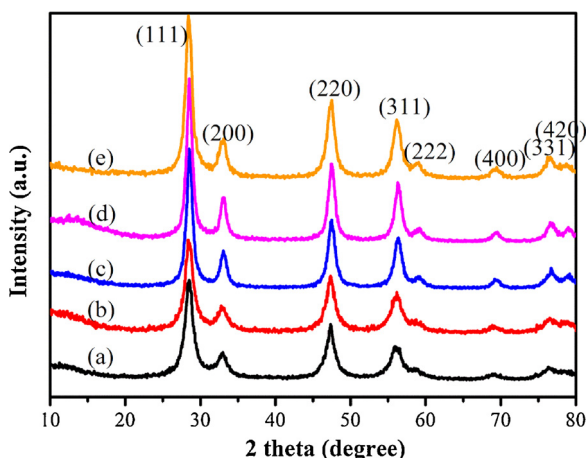


Fig. 2. XRD patterns for (a) CeO_2 , (b) $\text{CeO}_2\text{-P}$, (c) $\text{Pt}/(\text{CeO}_2\text{-P})$, (d) Pt/CeO_2 and (e) $(\text{Pt}/\text{CeO}_2)\text{-P}$ catalysts.

2.4. Stability and water resistance test

The water resistance of the catalysts was tested with the same concentration (200 ppm) and flow rate (100 ml min^{-1}) of toluene reacted for 50 h and their stability evaluated for 10–15 h with 9.6-vol% water vapor. Next, the water resistance of the catalysts was tested under increased humidity conditions of 5–20 vol% water vapor, which was achieved by bubbling the water with pure N_2 and mixing with an O_2 flow at 30°C in the incubator and holding for 60 min per humidity point.

3. Results and discussion

3.1. Effect of plasma on structure and morphology of catalyst

3.1.1. Crystal structure

Fig. 2 shows the XRD patterns of the CeO_2 and Pt/CeO_2 catalysts with and without plasma treatment. Each spectrum exhibited well-resolved diffraction peaks, which were indexed to the (111), (200), (220), (311), (222), (400), (331), and (420) planes that are characteristic of the face-centered cubic fluorite structure with space group $Fm\bar{3}m$ (JCPDS Card No. 34-0394) [28]. The loading of Pt caused a slight shift in the diffraction peaks, which shifted to higher angles relative to the peaks of the CeO_2 due to an extension of the framework accompanied by an increased mean crystal size. The mean crystal sizes were calculated using the Scherrer formula and are summarized in Table 1. There is no diffraction peak of Pt or PtO_x phase (at approximately 40°), which probably was due to the low loading content, 0.77–0.88 wt %, of

$\text{Pt} \leq 1.0$ wt%. Hence, there is no obvious effect on the mean crystal size of CeO_2 -based catalysts by DBD plasma treatment.

3.1.2. Surface roughness

The STEM images show that the CeO_2 -based catalysts both with and without Pt NPs have high uniformity and well-defined morphologies (Fig. 3a–e). Fig. 3a1–e1 show the detailed shape and crystal facets of the CeO_2 nanostructures for all catalysts, in which lattice fringes are clearly observed over a large area, corresponding to the (111), (200), and (220) planes of cubic CeO_2 . The clear lattice images indicate the good crystallinity and single crystalline nature of the CeO_2 nanorods, and no impact on the crystallinity size by discharge. Fig. 3a and b show TEM images of CeO_2 and $\text{CeO}_2\text{-P}$ catalysts, respectively, and that the partial CeO_2 nanorods were broken after plasma treatment. The size of CeO_2 with discharge became remarkably shorter than they were before discharge. The intensity of STEM images was measured by using an adjacent CeO_2 nanorod as a reference, to display the roughness of the catalyst surface [29]. Fig. 3a2 and b2 show the surface roughness of CeO_2 and $\text{CeO}_2\text{-P}$, and the formation of more and larger notches of $\text{CeO}_2\text{-P}$ that provide strong and direct evidence that the surface of $\text{CeO}_2\text{-P}$ is rougher than that of CeO_2 . This is probably because the catalysts were etched by the reactive ions during plasma discharge [30], which created more roughness on the surface of catalysts. In addition, the fraction of rather energetic ions may potentially influence the surface morphology [31]. Guo et al. [32] found similar phenomena, namely rough or porous crystal surfaces after the plasma catalysis reaction of oxygen content in air and at atmosphere pressure with DBD plasma.

3.1.3. Pt NP size and dispersion

To study of the effect of plasma on the size of Pt NPs on the surface of CeO_2 nanorods, the Pt NPs were distinguished from the CeO_2 support in the images shown in Fig. 3c, c1, d, d1, e and e1; the corresponding diameters and dispersions were calculated and are summarized in Table 1. Assuming that the Pt NPs are spherical, the diameters of a Pt NP can be approximately determined based on its distance [29]. Accordingly, we randomly examined over 50 Pt NPs and the statistics show that the NP sizes range from 1.5 to 6.0 nm (Fig. 3c3, d3, e3). The average Pt NP sizes ($d_{1\text{pt}}$) of $\text{Pt}/(\text{CeO}_2\text{-P})$, Pt/CeO_2 and $(\text{Pt}/\text{CeO}_2)\text{-P}$ are 3.55, 3.34, and 3.27 nm, respectively. The catalysts upon loading after discharge decreased the size of Pt NPs, while loading before discharge increased their size. The dispersions of Pt NPs ($D_{1\text{pt}}$) calculated by the Pt NP sizes determined from TEM images are 31.67% [$\text{Pt}/(\text{CeO}_2\text{-P})$], 33.66% (Pt/CeO_2) and 34.38% [$(\text{Pt}/\text{CeO}_2)\text{-P}$], respectively. Moreover, the NP sizes ($d_{2\text{pt}}$) based on CO chemisorption measurements are the same, in the following order: $\text{Pt}/(\text{CeO}_2\text{-P})$ (4.41 nm), Pt/CeO_2 (4.05 nm) and $(\text{Pt}/\text{CeO}_2)\text{-P}$ (3.87 nm), and the calculated sizes of all catalysts are

Table 1
Structural properties of various samples.

Catalysts	^a Pt loading (wt.%)	^b Surface area ($\text{m}^2 \text{ g}^{-1}$)	^c Nanorod size (D × L) (nm)	^d Mean crystal Size (nm)	Pt particle size (nm) ^e $d_1 \text{--} d_2$	Dispersion (%) ^e $D_1 \text{--} D_2$
CeO_2	–	85.2 ± 0.4	$12 \pm 5 \times 150 \pm 50$	10	–	–
$\text{CeO}_2\text{-P}$	–	95.7 ± 0.8	$12 \pm 5 \times 100 \pm 50$	10	–	–
$\text{Pt}/(\text{CeO}_2\text{-P})$	0.88	85.9 ± 0.4	$13 \pm 5 \times 100 \pm 50$	11	3.55	4.41
Pt/CeO_2	0.77	82.1 ± 0.3	$13 \pm 5 \times 120 \pm 50$	11	3.34	4.05
$(\text{Pt}/\text{CeO}_2)\text{-P}$	0.77	87.1 ± 0.2	$13 \pm 5 \times 100 \pm 50$	11	3.27	3.87

Note: all samples were reduced.

^a Determined by ICP-AAS.

^b Surface area determined from N_2 isotherm.

^c Evaluated for approximately 100 nanorods from TEM images.

^d Estimated by the Scherrer equation, applied to the (111) reflection on fluorite CeO_2 .

^e Diameter of the loading Pt NPs obtained from TEM images.

^f Diameter of the loading Pt NPs measured by CO chemisorption, conducted at 303 K.

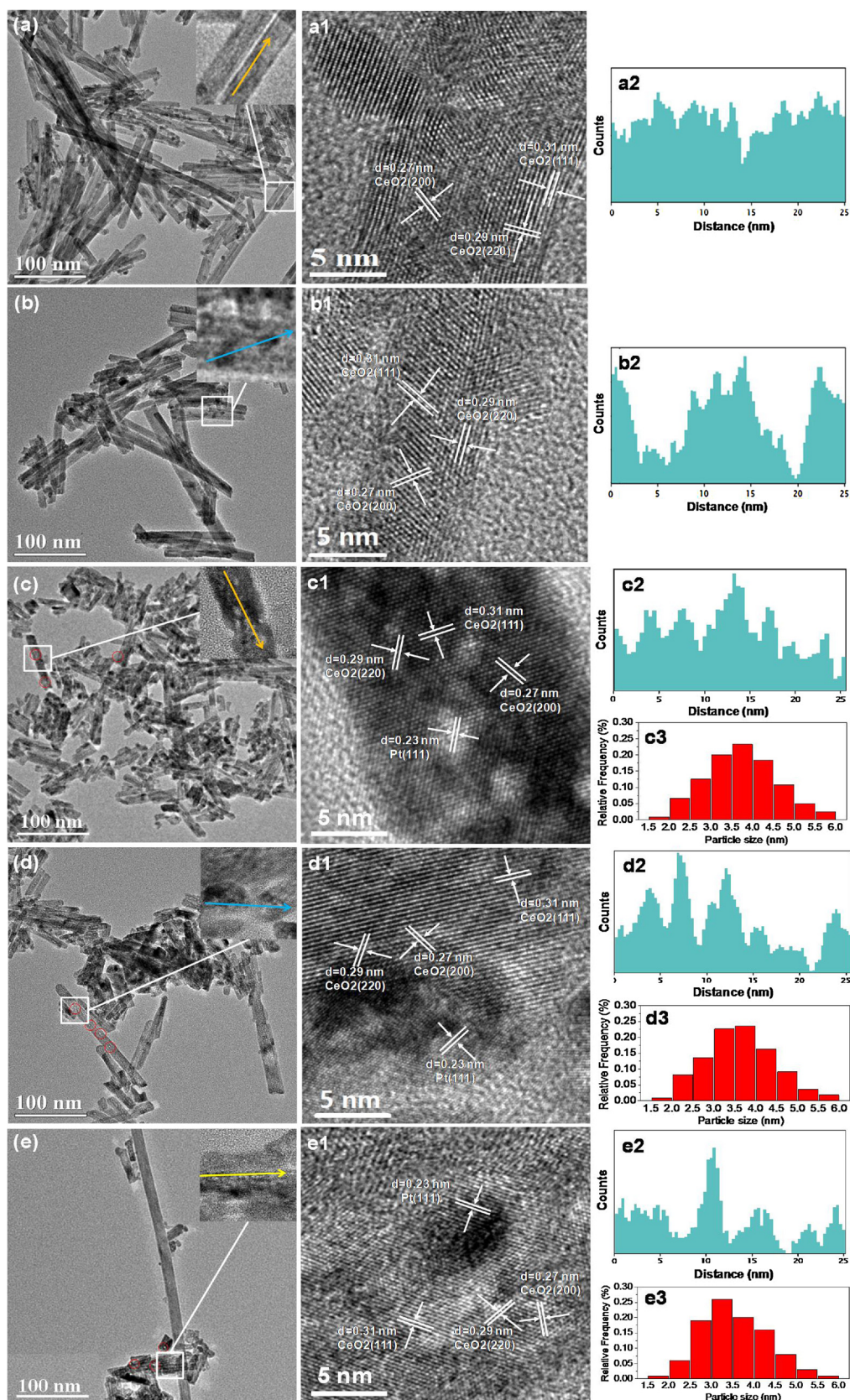


Fig. 3. STEM image analysis of CeO₂ (a, a1, and a2), CeO₂-P (b, b1, and b2), Pt/(CeO₂-P) (c, c1–c3), Pt/CeO₂ (d, d1–d3) and (Pt/CeO₂)-P (e, e1–e3) catalysts.

larger than those from the statistical analysis results from TEM images. These results are consistent with those in Ref. [33]. The surfaces of Pt/(CeO₂-P) were rougher and the Pt NPs were larger owing to the

aggregation of Pt NPs at a nearby notch, which then formed more larger-sized Pt NPs, while the Pt NPs of (Pt/CeO₂)-P were smaller compared with Pt/CeO₂. The reduction process can modify the Pt

particle size, and thus the Pt size data of unreduced catalyst are presented in Table S2 and Fig. S3. The Pt particles grew (increment < 0.15 nm) after reduction, while the effects of the plasma still existed for unreduced catalysts. Fig. 3d and e, it can be seen that several smaller NPs of nearly the same size may have broken off from the larger ones (clusters), which were recombined by high energetic species and then dispersed well. The plasma was usually introduced to age the catalyst in air and atmospheric-pressure conditions by high energetic electrons [30]. Therefore, the Pt atom of Pt/CeO₂ might be recombined via bombardment by energetic electrons to form smaller Pt particles. Hatano et al. [34] also believe that the agglomerated Pt particles would be redispersed under an oxidative atmosphere as well. Based on the above literature conclusions that the high energetic electrons may play an important role in plasma treatment. In addition to high energetic electron, the reactive ions and active radicals with kinetic energy might have also played a role in the plasma treatment process [30,31]. The same results were obtained by Guo et al. [32] that the detection of smaller particles of active components on the surface of catalysts after plasma catalysis reaction in dry air and atmospheric pressure using DBD plasma. Therefore, it is shown that the DBD plasma has a significant impact on the dispersion and size of Pt NPs loaded on CeO₂ catalysts.

3.1.4. Specific surface area and pore distribution

The N₂ isotherms and pore size distribution plot of the CeO₂-based catalysts were examined using N₂ physisorption measurements (Fig. 4). The textural properties obtained from the N₂ physisorption measurements are summarized in Table 1. All of the curves exhibited type-IV adsorption isotherms (Fig. 4a and b). A type-H2 hysteresis loop with a sloping adsorption branch and a triangular sharp, steep desorption branch was observed at the relative pressure (P/P₀) for all catalysts. This behavior was attributed to the pore connectivity effects, which were often considered to be a result of the presence of pores with narrow mouths (ink-bottle pores) [35]. The pore size distributions of all the samples, which were calculated from the N₂ adsorption isotherms using the BJH adsorption branch. For catalysts of pure CeO₂ without Pt NPs, the presence of same hysteresis loop suggests that the natural

structure of catalysts remained even after plasma treatment. A type-H2 hysteresis loop at relatively high pressure (P/P₀) and the pore distribution curve suggests that a large number of the gap holes or narrow holes formed by the accumulation of nanorods existed in the CeO₂ nanorod (Fig. 4a and c). Compared with the pure CeO₂ catalyst, the BET surface areas of CeO₂-P were increased 10.5 m² g⁻¹ after plasma treatment. The pore size of the plasma treated CeO₂-P (2.6 nm) was slightly larger than that of the untreated CeO₂ and is mainly centered at 2.3 nm (Fig. 4c). The reasons for the changes in the BET surface areas and pore sizes is the more and larger notches on the surfaces of the catalysts (Fig. 3b2) and the broken nanorods (Fig. 3b). The broken nanorods might be cause of the thermal stress [36,37], and the heating by high energy electrons [38].

Compared with pure CeO₂, the surface area of Pt/CeO₂ decreased 13.6 m² g⁻¹ because the surface pores were filled by the Pt NPs. The BET surface areas of the Pt/CeO₂ catalysts slightly increased before and after the loading of Pt by the plasma treatment (Table 1). For the catalysts of CeO₂ with Pt NPs, the presence of same hysteresis loop suggests that the pore structure of the catalysts remained after the plasma treatment (Fig. 4b). However, the position of the hysteresis loop shifted to a low position compared with that of the pure CeO₂. This shows that the number of CeO₂ catalysts with Pt NPs with surface notches (1.7–4.0 nm) and narrow holes (4.0–20 nm) had changed; that is, the former decreased and the latter increased based on the pore-distribution curve (Fig. 4d). By comparing the results with and without discharge, we determined that the uniform order of pore distribution of the CeO₂-based catalysts is as follows: (Pt/CeO₂)-P > Pt/CeO₂ > Pt/(CeO₂-P) (Fig. 4d). The pore size of the (Pt/CeO₂)-P catalyst was slightly smaller than that of the Pt/CeO₂ catalyst, mainly centered at 2.0 nm, of which the quantity increased. The reason for the poor uniform pore distribution of Pt/(CeO₂-P) was that the larger size of the notches led to a greater number of Pt aggregated, and the formation of larger Pt NPs (Fig. 3c2), resulting in a decrease surface area and a increase in the number of gap holes.

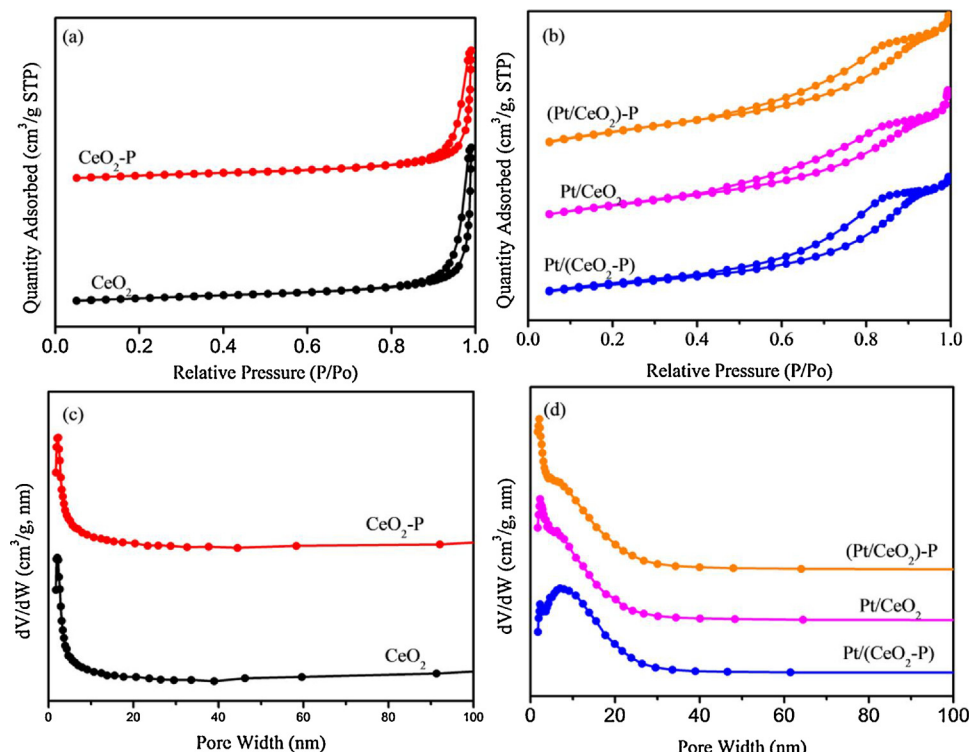


Fig. 4. (a and b) N₂ adsorption-desorption measurements for all samples; (c and d) pore size distributions of all samples.

Table 2

Relative intensities of different Ce, O and Pt species as observed from the XPS spectra and relative concentration of oxygen vacancies from UV-Raman spectra.

Catalysts	$\text{Pt}^\circ/(\text{Pt}^{2+} + \text{Pt}^\circ)$	$\text{Ce}^{3+}/(\text{Ce}^{3+} + \text{Ce}^{4+})$	$\text{O}_{\text{Sur}}/(\text{O}_{\text{Sur}} + \text{O}_{\text{Lat}})$	I_D/I_{F2g}
	(%)	(%)	(%)	
CeO_2	–	30.30	34.71	0.93
$\text{CeO}_2\text{-P}$	–	31.20	36.85	1.19
$\text{Pt}/(\text{CeO}_2\text{-P})$	79.14	33.00	34.68	1.88
Pt/CeO_2	75.00	31.90	33.30	1.47
$(\text{Pt}/\text{CeO}_2)\text{-P}$	79.17	33.11	41.94	2.19

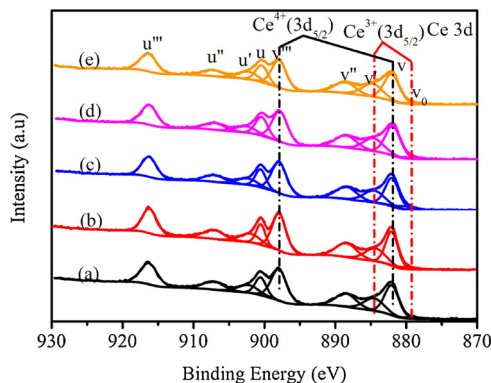


Fig. 5. XPS spectra of Ce 3d peaks for all catalysts: (a) CeO_2 , (b) $\text{CeO}_2\text{-P}$, (c) $\text{Pt}/(\text{CeO}_2\text{-P})$, (d) Pt/CeO_2 and (e) $(\text{Pt}/\text{CeO}_2)\text{-P}$ catalysts.

3.2. Effect of plasma on chemical properties of catalyst

3.2.1. Active components and chemical states

The characterization of chemical species of the Ce, O and Pt located in the surface region of the catalysts was detected by XPS, and the values of different species of Ce, O and Pt from the deconvoluted peak area were calculated and are summarized in Table 2. As shown in Fig. 5, Ce 3d XPS of CeO_2 both with Pt and without Pt NPs shows the characteristic main and satellite peaks due to Ce^{4+} and Ce^{3+} oxidation states [39,40]. v' , v'' , v''' , u' , u'' , and u''' were assigned to the characteristic peaks of the Ce^{4+} oxidation state. The other three characteristic peaks u' , v_0 and v' could be assigned to the Ce^{3+} oxidation state, which would generally serve as an indicator of the existence of oxygen vacancies on the ceria surface. Ce 3d XPS data indicated that the Ce^{4+} oxidation state mainly exists in the CeO_2 and Pt/CeO_2 systems. The plasma treated catalysts have a higher Ce^{3+} proportion [$\text{CeO}_2\text{-P}$, 31.20%; $\text{Pt}/(\text{CeO}_2\text{-P})$, 33.00%; $(\text{Pt}/\text{CeO}_2)\text{-P}$, 33.11%] than the untreated catalysts (CeO_2 , 30.30%; Pt/CeO_2 , 31.90%), indicating a higher concentration of oxygen vacancies via plasma discharge. This result is in close agreement with the concentration of oxygen vacancies (I_D/I_{F2g}) detected by UV-Raman spectroscopy (Table 3). Regarding the oxygen in the catalyst, the O 1s spectra exhibit three features as shown in Fig. 6. The peak at

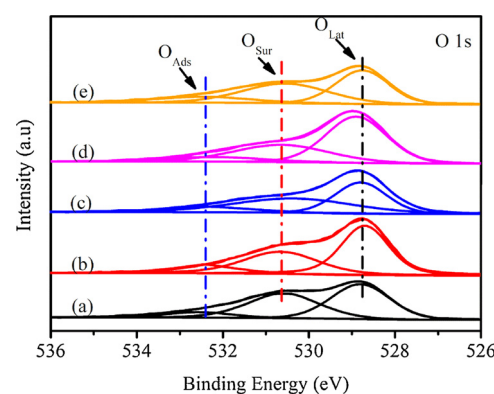


Fig. 6. XPS spectra of O 1s peaks for all catalysts: (a) CeO_2 , (b) $\text{CeO}_2\text{-P}$, (c) $\text{Pt}/(\text{CeO}_2\text{-P})$, (d) Pt/CeO_2 and (e) $(\text{Pt}/\text{CeO}_2)\text{-P}$ catalysts.

lower binding energy (528.7–528.9 eV) corresponds to lattice oxygen (O^{2-}), whereas the next peak (530.4–530.7 eV) is assigned to the surface oxygen (O_2^{2-} or O^-). The form of hydroxyl OH^- carbonate CO_3^{2-} species and adsorbed molecular water is regarded as adsorption oxygen (above 532.0 eV) [24]. It is very clear that the plasma-treated $\text{CeO}_2\text{-P}$, $\text{Pt}/(\text{CeO}_2\text{-P})$ and $(\text{Pt}/\text{CeO}_2)\text{-P}$ catalysts contained more surface oxygen (O_2^{2-} or O^-) compared to CeO_2 and Pt/CeO_2 . The increased amounts of surface oxygen were 1.14%, 1.38% and 8.64%, respectively. More surface oxygen in the catalysts would make it easier to oxidize toluene [41]. Fig. 7 presents the XPS spectra of Pt 4f peaks. The Pt 4f_{7/2} peak can be deconvoluted into two peaks at 71.6–71.9 and 72.6–72.9 eV, and the Pt 4f_{5/2} peak can also be deconvoluted into two peaks at 75.0–75.3 and 76.1–76.4 eV [21]. The peaks at 71.6–71.9 and 75.0–75.2 eV are assigned to the Pt° species. Upon undergoing the discharge treatment, the ratio of Pt° shows an increase of 4.14% and 4.17 for $\text{Pt}/(\text{CeO}_2\text{-P})$ and $(\text{Pt}/\text{CeO}_2)\text{-P}$, respectively. It is noticeable that the plasma-treated catalysts with Pt NPs possessed greater amounts of Pt° , which provide active sites [21]. Regarding the above-mentioned results, the catalysts loaded with Pt NPs after discharge exhibited the higher proportions of Ce^{3+} , O_{surf} , and Pt° . It is thus concluded that plasma discharge changes the oxidation state of Ce and Pt, the same phenomenon reported in previous research [16].

3.2.2. Oxygen vacancies

The UV-Raman spectra of all the CeO_2 and Pt/CeO_2 catalysts are displayed in Fig. 8, and are normalized with respect to the Raman signal at ~ 460 and $\sim 590 \text{ cm}^{-1}$. All samples were reduced before characterization. According to previous studies [42,43], the main peak at $\sim 460 \text{ cm}^{-1}$ can be attributed to the triply degenerate F_{2g} mode of CeO_2 with fluorite structure, while the peaks at $\sim 590 \text{ cm}^{-1}$ can be assigned to the defect induced (D) mode that is connected to the oxygen

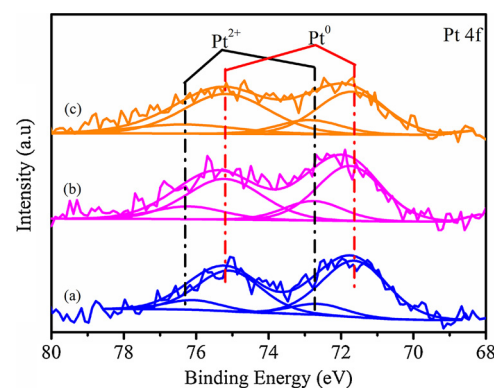


Fig. 7. XPS spectra of Pt 4f peaks for all catalysts: (a) $\text{Pt}/(\text{CeO}_2\text{-P})$, (b) Pt/CeO_2 and (c) $(\text{Pt}/\text{CeO}_2)\text{-P}$ catalysts.

Table 3

H_2 temperature-programmed reduction and O_2 temperature-programmed desorption data for catalysts.

Catalysts	H ₂ -TPR		O ₂ -TPD	
	Peak positions (°C)	H ₂ consumption ($\mu\text{mol g}^{-1}$)	Peak positions (°C)	Desorption amount ($\mu\text{mol O g}^{-1}$)
CeO_2	395	277	104, 330	149, 50
$\text{CeO}_2\text{-P}$	343, 422	207, 74	109, 332	162, 58
$\text{Pt}/(\text{CeO}_2\text{-P})$	83, 169, 401	14, 219, 121	102, 256	168, 113
Pt/CeO_2	94, 188, 417	12, 157, 134	95, 232	159, 91
$(\text{Pt}/\text{CeO}_2)\text{-P}$	117, 370	87, 280	98, 238	233, 105

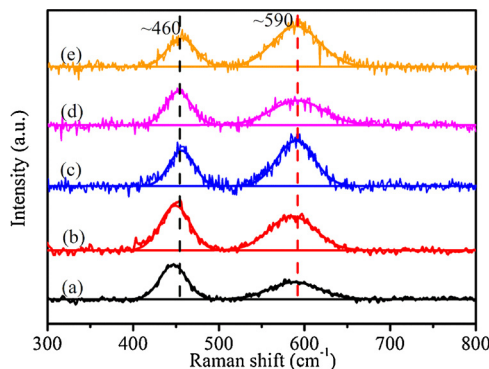


Fig. 8. UV-Raman spectra of (a) CeO_2 , (b) $\text{CeO}_2\text{-P}$, (c) $\text{Pt}/(\text{CeO}_2\text{-P})$, (d) Pt/CeO_2 and (e) $(\text{Pt}/\text{CeO}_2)\text{-P}$ catalysts.

vacancies induced by the existence of the Ce^{3+} ions of CeO_2 [35]. The relative ratio of I_D/I_{F2g} represents the relative concentration of oxygen vacancies [40]. When Pt was impregnated on ceria, those UV-Raman peaks still remained and the peak positions exhibited no obvious shift, but the I_D/I_{F2g} ratios increased in the following order: CeO_2 ($I_D/I_{F2g} = 0.93$), $\text{CeO}_2\text{-P}$ ($I_D/I_{F2g} = 1.19$), Pt/CeO_2 ($I_D/I_{F2g} = 1.47$), $\text{Pt}/(\text{CeO}_2\text{-P})$ ($I_D/I_{F2g} = 1.88$) and $(\text{Pt}/\text{CeO}_2)\text{-P}$ ($I_D/I_{F2g} = 2.19$), as shown in Table 2. The oxygen vacancy concentrations of the unreduced catalysts are presented in Table S2 and Fig. S4. The concentration of the oxygen vacancies were changed by the reduction process, while the change was slightly increased (< 0.2) after reduction. The effects of plasma treatment still exist for the unreduced catalysts as well. After plasma treatment, the catalysts presented more oxygen vacancies. As the formation of oxygen vacancy was related to neutral oxygen localize on f states of CeO_2 [44], therefore, the energetic electron bombardment might change the electron distribution or atomic scale structure disorder [45] and form oxygen vacancies. The oxygen has high mobility in CeO_2 , the O_2/N_2 plasma produced oxygen reactive species also contributed to the formation of the oxygen vacancy. Hence, the energetic electron bombardment and oxygen reactive species might play an important role in oxygen vacancy creation. Chae et al. [46] attributed the formation of oxygen vacancies and Ti^{3+} ions to the collisions and sputtering of energetic species during plasma treatment. The authors of Ref. [47] reported similar results that the lower-valence manganese oxide (Mn_3O_4) was detected after plasma catalysis. More direct evidence is needed to illustrate the phenomenon, as are further studies of the detailed mechanism that produces more oxygen vacancies in DBD plasma treatment.

3.2.3. H_2 reducibility and oxygen desorption property

H_2 -TPR profiles of all catalysts are shown in Fig. 9, and the H_2

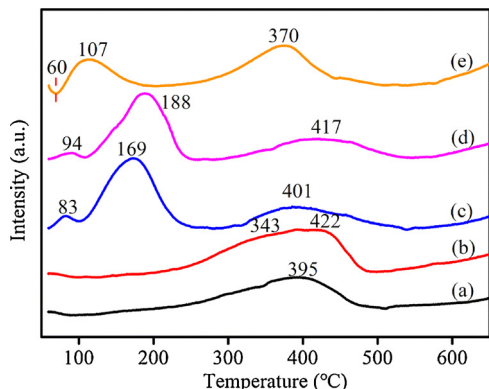


Fig. 9. H_2 temperature-programmed reduction curves of (a) CeO_2 , (b) $\text{CeO}_2\text{-P}$, (c) $\text{Pt}/(\text{CeO}_2\text{-P})$, (d) Pt/CeO_2 and (e) $(\text{Pt}/\text{CeO}_2)\text{-P}$ catalysts.

consumption values are reported in Table 3. One reduction peak at ~ 395 °C can be observed on the pure CeO_2 sample that originated from the reduction of the surface and sub-surface of CeO_2 [48]. After plasma treatment of CeO_2 , two reduction peaks (343 °C and 422 °C) appeared and consumed more H_2 . When Pt was impregnated on CeO_2 , three reduction peaks appeared at below 100 °C, at 100 °C– 250 °C, and 250 °C– 500 °C, which could be assigned to the reduction of oxygen from PtOx , and Pt-O-Ce on both the surface and sub-surface of CeO_2 , respectively [40,49]. The reduction peaks of Pt/CeO_2 catalysts after plasma treatment decreased. The small peak position below 100 °C present as a shoulder in the TPR profiles of Pt/CeO_2 (94 °C) and $\text{Pt}/(\text{CeO}_2\text{-P})$ (83 °C), while that of $(\text{Pt}/\text{CeO}_2)\text{-P}$ appeared as a negative peak at lower temperature (60 °C), formed by the adsorption of H_2 from the Pt° , which was generated by plasma treatment. This explanation is suggested by the previous results of increased Pt° ratio elicited by XPS analysis (see Table 2). A second apparent peak position at 100 °C– 250 °C indicates the presence of Pt-O-Ce species formed by the strong interaction between Pt and CeO_2 [50,51]. It is widely accepted that Pt spills over H to the neighboring CeO_2 surface, which subsequently facilitates the reduction of the CeO_2 surface at lower temperature [24]. The effect of plasma on Pt-O-Ce catalyst is obvious for temperatures from 188 °C down to 169 °C and 117 °C. Higher-temperature ($T > 300$ °C) peaks are observed in the following order: Pt/CeO_2 (417 °C), $\text{Pt}/(\text{CeO}_2\text{-P})$ (401 °C) and $(\text{Pt}/\text{CeO}_2)\text{-P}$ (370 °C). Note that the observed H_2 consumptions below 200 °C on Pt/CeO_2 (169 $\mu\text{mol/g}$) $\text{Pt}/(\text{CeO}_2\text{-P})$ (233 $\mu\text{mol g}^{-1}$) and $(\text{Pt}/\text{CeO}_2)\text{-P}$ (87 $\mu\text{mol g}^{-1}$) are significantly larger than the value of the Pt loaded ($20 \mu\text{mol g}^{-1}$). This result also supports the fact that not only does PtOx react with H_2 below 200 °C, but also that the Pt-O-Ce surface oxygen of CeO_2 gives rise to the formation of metallic Pt and surface oxygen vacancies. Therefore, we can say that plasma treatment has an effect on dispersed Pt and a strong interaction between PtOx and CeO_2 .

Fig. S1 shows the O_2 -TPD curves of all catalysts, and Table 3 reports the values of O_2 consumption. It can be seen from the figure that two desorption peaks of oxygen species can be identified O_2^- (ad) or O_2^{2-} (ad) (~ 100 °C) and O^- (surf) (200 °C– 400 °C) [35,48]. Compared with CeO_2 , the O^- (surf) of Pt/CeO_2 samples had a lower desorption temperature and greater amount of desorbed O_2 . In addition, a slightly increased temperature and O_2 adsorption amount was observed on $\text{CeO}_2\text{-P}$ compared with CeO_2 . More low-temperature O_2 desorption is observed on Pt/CeO_2 , while more O_2 desorbs on $\text{Pt}/(\text{CeO}_2\text{-P})$ and $(\text{Pt}/\text{CeO}_2)\text{-P}$, and the $(\text{Pt}/\text{CeO}_2)\text{-P}$ amount increases most and most significantly. The evidence indicates that with the plasma treatment, Pt/CeO_2 has a significant effect on O_2 desorption. This is consistent with the H_2 -TPR data for which more active oxygen species are generated on the surface by the plasma treatment.

3.3. Effect of plasma on activities of catalyst

3.3.1. Activities evaluation

The activities of various CeO_2 and Pt/CeO_2 catalysts were measured and compared by evaluating the catalytic oxidation reactions of toluene. Conversions of toluene to CO_2 are shown in Fig. 10. The temperatures for conversion of toluene oxidized to CO_2 concentrations of 50% (T_{50}) and 90% (T_{90}) are listed in Table 4, and the conversion of toluene to non-toluene and selectivity of CO_2 are displayed in Table S1. The T_{90} values of toluene conversions to CO_2 for the various catalysts with and without Pt NPs decreased in the following order: CeO_2 and $\text{CeO}_2\text{-P}$ ($T_{90} > 300$ °C), Pt/CeO_2 ($T_{90} = 287$ °C), $\text{Pt}/(\text{CeO}_2\text{-P})$ ($T_{90} = 273$ °C), and $(\text{Pt}/\text{CeO}_2)\text{-P}$ ($T_{90} = 208$ °C). The T_{90} value of $\text{CeO}_2\text{-P}$ slightly decreased compared with pure CeO_2 , and the T_{90} values of various Pt/CeO_2 catalysts were lower than those of CeO_2 without Pt NPs; in other words the various Pt/CeO_2 catalysts exhibited higher activities than CeO_2 without Pt NPs. Among the catalysts, $(\text{Pt}/\text{CeO}_2)\text{-P}$ showed the best catalytic activity and a T_{90} temperature much lower than that of Pt/CeO_2 and $\text{Pt}/(\text{CeO}_2\text{-P})$. The changed activities of

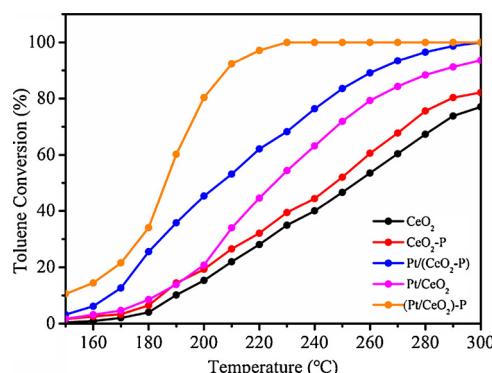


Fig. 10. Conversion of toluene to CO_2 for various CeO_2 and Pt/CeO_2 catalysts.

Table 4
Catalytic performances of catalysts.

Catalysts	Catalytic activity		^a TOF _{Pt} (10^{-4} s^{-1})	^a TOF _{Ov} (10^{-5} s^{-1})	^b Ea (kJ mol ⁻¹)
	T ₅₀ (°C)	T ₉₀ (°C)			
CeO_2	255	> 300	–	0.62	–
$\text{CeO}_2\text{-P}$	247	> 300	–	1.90	–
$\text{Pt}/(\text{CeO}_2\text{-P})$	206	262	2.79	3.38	69.8
Pt/CeO_2	225	287	2.62	2.67	79.1
$(\text{Pt}/\text{CeO}_2)\text{-P}$	185	208	9.88	9.49	63.8

^a Calculated at 150 °C.

^b Calculated at lower than 10% toluene conversion and determined by the Arrhenius plot.

catalysts were related to the plasma treatment. In general, the exposed Pt atoms are regarded as active sites that could strongly adsorb toluene molecules and activate them into dehydrogenated intermediates [52]. Upon undergoing plasma treatment, $(\text{Pt}/\text{CeO}_2)\text{-P}$ processed smaller Pt NPs (higher dispersion) and exposed more Pt atoms on the surface that contribute to the catalytic performance. Another important reason for this may be the increased concentration of oxygen vacancies, which were also regarded as reactive sites and affected the catalytic activity in re-oxidations [9,42]. The Raman spectroscopy, O_2 -pulse and XPS results indicate that $(\text{Pt}/\text{CeO}_2)\text{-P}$ has the most oxygen vacancy. In Ref. [24], it was considered that the oxidation of toluene on Pt/CeO_2 obeys the Mars-van-Krevelen mechanism, including the reduction of the oxidized catalyst by the toluene and the oxidation of the catalyst by oxygen from the gaseous phase. The H_2 -TPR and O_2 -TPD results also demonstrate that $(\text{Pt}/\text{CeO}_2)\text{-P}$ has good reducibility and O-desorption ability, which is important and useful to enhancing catalytic performance. In addition, the larger surface area (more rough surface) of $(\text{Pt}/\text{CeO}_2)\text{-P}$ also proved useful in enhancing catalytic performance [53]. In summary, the results of catalyst characterization were consistent with the increased activity of $(\text{Pt}/\text{CeO}_2)\text{-P}$ upon plasma treatment. To better understand the origin of the increased catalytic activity induced by plasma treatment, the activation energies (Ea) and turnover frequency (TOF_{Pt} and TOF_{Ov}) were calculated.

3.3.2. Activation energies

Arrhenius plots provide the apparent activation energies for toluene oxidation on CeO_2 -based with Pt NPs catalysts, as shown in Fig. 11. From the Arrhenius plots of the rate constant k over CeO_2 -based catalysts obtained in the range 388–423 K with low conversion (< 10%), the apparent activation energies for oxidation of toluene on the Pt loading catalysts were calculated to be in the following order: Pt/CeO_2 (79.1 kJ mol⁻¹), $\text{Pt}/(\text{CeO}_2\text{-P})$ (69.8 kJ mol⁻¹) and $(\text{Pt}/\text{CeO}_2)\text{-P}$ (63.8 kJ mol⁻¹) (see Table 4). The lower the Ea value, the easier it is to activate and oxidation of toluene; this Ea result is in accordance with the

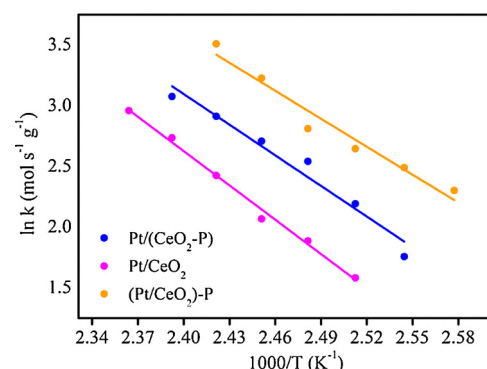


Fig. 11. Arrhenius plots of toluene oxidation for all Pt/CeO_2 catalysts.

evaluation of toluene oxidation and indicates that Pt/CeO_2 after plasma treatment with the lowest activation energies also exhibits the highest toluene oxidation activity.

3.3.3. Turnover frequency

More active sites were exposed with larger specific surface area and higher dispersion of the catalysts, which is more conducive to the oxidation of pollutants. Even though result of this study shows that the surface area of $\text{CeO}_2\text{-P}$ increased more than that of pure CeO_2 , the activities were slightly increased; moreover, it was further indicated that the surface area of Pt loaded on CeO_2 were slightly increased by the plasma treatment. Hence, we suggest that the surface area had a slight influence on the reaction rate in this study. In general, the exposed Pt atoms of the catalyst are considered the active sites, which could strongly adsorb toluene molecules and then activate them into dehydrogenated intermediates as well as dissociative oxygen [8,54]. Therefore, the turnover frequency of Pt NPs (TOF_{Pt}) could be the rate-determining factor for toluene oxidation. In order to estimate TOF_{Pt}, the number of available or exposed Pt sites for reactions was detected by CO pulse chemisorption measurements at 30 °C; the results are summarized in Table 4. The TOF_{Pt} values of various Pt/CeO_2 catalysts showed a significant difference and decreased in the order Pt/CeO_2 ($2.62 \times 10^{-4} \text{ s}^{-1}$), $\text{Pt}/(\text{CeO}_2\text{-P})$ ($2.79 \times 10^{-4} \text{ s}^{-1}$), and $(\text{Pt}/\text{CeO}_2)\text{-P}$ ($9.88 \times 10^{-4} \text{ s}^{-1}$). The result of the size and dispersion of Pt NPs was not corrected by the TOF_{Pt} values for various Pt/CeO_2 catalysts. This suggests that exposed Pt atoms are not the sole active site of species. This conclusion is consistent with previous studies [28]. CeO_2 possesses rich oxygen vacancies that play an important role in toluene oxidation [24], specifically by replenishing active oxygen species and accelerating oxygen cycle from gas to lattice. The concentration of oxygen vacancy was determined by O_2 pulse chemisorption, and the OSC_{surf} value is regarded as the amount of oxygen consumption by oxygen vacancies on the CeO_2 surface [28,55]. The TOF_{Ov} values were then calculated according to the concentration of oxygen vacancies and the results are presented in Table 4. Their order was consistent with that of the TOF_{Pt} values: CeO_2 ($0.62 \times 10^{-5} \text{ s}^{-1}$), $\text{CeO}_2\text{-P}$ ($1.90 \times 10^{-5} \text{ s}^{-1}$), Pt/CeO_2 ($2.67 \times 10^{-5} \text{ s}^{-1}$), $\text{Pt}/(\text{CeO}_2\text{-P})$ ($3.38 \times 10^{-5} \text{ s}^{-1}$), and $(\text{Pt}/\text{CeO}_2)\text{-P}$ ($9.49 \times 10^{-5} \text{ s}^{-1}$). These values agreed with the catalytic performance, and indicate that the oxygen vacancies are also one of the active sites.

The TOF_{Pt} value of $\text{Pt}/(\text{CeO}_2\text{-P})$ is lower than that of Pt/CeO_2 , which is the reason that the number of available Pt atoms of $\text{Pt}/(\text{CeO}_2\text{-P})$ (1.02×10^{18} atoms) was higher than Pt/CeO_2 (0.92×10^{18} atoms). As a result, the same quality of catalyst, $\text{Pt}/(\text{CeO}_2\text{-P})$, exhibited higher activity. The increased TOF_{Pt} and TOF_{Ov} values of $\text{Pt}/(\text{CeO}_2\text{-P})$ and $(\text{Pt}/\text{CeO}_2)\text{-P}$ could be attributed to the plasma treatment, which impacts the electrons of the Ce and Pt molecules, changes the bond length or energies, then enhances the strong interaction between Pt and CeO_2 , and finally increases the catalytic activity [56]. The above results clearly indicate that DBD plasma treatment can effectively promote catalytic

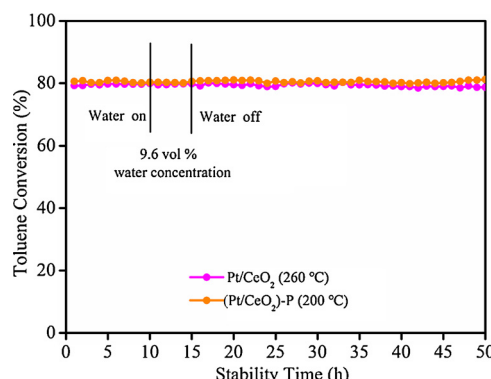


Fig. 12. Stability and water-resistance test results during 50 h of toluene oxidation.

activity and enhance the strong interaction between Pt and CeO₂. This may be able to explain that ceria is able to spillover atomic oxygen to neighboring Pt, where toluene is absorbed and bonded [22,57].

3.4. Effect of plasma on stability and water resistance of Pt/CeO₂ catalyst

3.4.1. Stability

The stability of the catalyst is an important factor in the practical application. Hence, the stability of Pt/CeO₂ and (Pt/CeO₂)-P catalysts was examined with consecutive catalytic runs and evaluation of the long-term catalytic performance of toluene oxidation. Durability tests of Pt/CeO₂ and (Pt/CeO₂)-P catalysts were set at 260 °C and 200 °C with a higher conversion of toluene to CO₂ (80%) over 50 h. As shown in Fig. 12, the toluene conversion of Pt/CeO₂ and (Pt/CeO₂)-P presented no obvious decrease during 50 h runs with a 200 ppm toluene concentration. The results indicate that the Pt/CeO₂ and (Pt/CeO₂)-P had good stability, which may be explained by the fact that carbon deposition on the surface can be effectively prevented by the high catalytic activity of loaded Pt particles and the thermal stability of CeO₂ [28,58]. In addition, the results in Table S1 indicate that the (Pt/CeO₂)-P with plasma treatment had a higher conversion of toluene and S_{CO2}, and formed fewer by-products that would be deposited on the surface of the catalyst. Wu et al. [59] also reported the same conclusion, namely that a higher carbon balance achieved with a plasma-treated catalyst indicates lower coke formation and better durability. The XRD patterns (Fig. 2) suggest that the crystal structure of (Pt/CeO₂)-P has not changed, and good thermal stability remains, also suggesting that (Pt/CeO₂)-P would still maintain good stability for toluene oxidation.

3.4.2. Water resistance

In order to understand the effect of humidity on toluene oxidation on the Pt/CeO₂ catalysts, and to reveal the catalytic performance under the simulated real exhaust conditions with water. The Fig. 12 shows the conversion of toluene to CO₂ with 9.6 vol% water vapor over the range 11–15 h. In short, there is no effect on toluene conversion. The effect of greater difference in humidity was also researched and the results shown in Fig. S2. With increasing humidity, the conversion of toluene to CO₂ slightly decreased, with the drop being lower than 3%. When the water was cut off, the toluene conversion was restored to its original value. These finding may indicate that mixing with a low (20 vol %) concentration of water vapor did not have a significant inhibitory effect on catalytic performance. The water is a by-product of toluene oxidation, and further, the oxygen molecules are adsorbed more facilely than water vapor so as to possess oxygen vacancies on CeO₂ at a relatively higher temperature (> 185 °C) [24,60].

4. Conclusions

A DBD plasma was introduced to modified CeO₂ and Pt/CeO₂ catalysts. The results of characterization and activities of these catalysts reveal that plasma has a significant impact on their structure and chemical properties, and also enhances the interaction between Pt and CeO₂. The increased surface areas were ascribed to broken CeO₂ nanorods and more and larger notches on the surface created by the plasma treatment. (Pt/CeO₂)-P exhibited the highest catalytic performance for toluene oxidation, which was attributed to a smaller size and higher dispersion of Pt NPs, possessed higher concentration of oxygen vacancies as observed by UV-Raman spectroscopy and XPS, presented higher TOF_{Pt} and TOF_{ov} values of 9.88×10^{-4} and $9.49 \times 10^{-5} \text{ s}^{-1}$, and lower activation energies of 63.8 kJ mol⁻¹. In addition, plasma-treated (Pt/CeO₂)-P still possessed excellent stability for toluene oxidation and water resistance. The details of plasma treatment mechanism remain unclear and require further studies.

Acknowledgements

This work is financially supported by the National Natural Science Foundation of China (No. 51378218, 51578245), the Fundamental Research Funds for the Central Universities, Natural Science Foundation of Guangdong Province, China (NO. 2015B020236002, 2016A030311003) and Science and Technology Program of Guangzhou (No. 201510010164). And we would like to thank LetPub ([www.letpub.com](http://www letpub.com)) for providing linguistic assistance during the preparation of this manuscript.

Appendix A. Supplementary data

Supplementary material related to this article can be found, in the online version, at doi:<https://doi.org/10.1016/j.apcatb.2018.07.044>.

References

- [1] N. Jiang, J. Hu, J. Li, K. Shang, N. Lu, Y. Wu, Plasma-catalytic degradation of benzene over Ag-Ce bimetallic oxide catalysts using hybrid surface/packed-bed discharge plasmas, *Appl. Catal. B: Environ.* 184 (2016) 355–363.
- [2] W. Xu, X. Xu, J. Wu, M. Fu, L. Chen, N. Wang, H. Xiao, X. Chen, D. Ye, Removal of toluene in adsorption-discharge plasma systems over a nickel modified SBA-15 catalyst, *RSC Adv.* 6 (2016) 104104–104111.
- [3] A. Vita, C. Italiano, C. Fabiano, L. Pino, M. Laganà, V. Recupero, Hydrogen-rich gas production by steam reforming of n-dodecane, *Appl. Catal. B: Environ.* 199 (2016) 350–360.
- [4] Y.X. Zeng, L. Wang, C.F. Wu, J.Q. Wang, B.X. Shen, X. Tu, Low temperature reforming of biogas over K-, Mg- and Ce-promoted Ni/Al₂O₃ catalysts for the production of hydrogen rich syngas: understanding the plasma-catalytic synergy, *Appl. Catal. B: Environ.* 224 (2018) 469–478.
- [5] X. Zhu, X. Gao, R. Qin, Y. Zeng, R. Qu, C. Zheng, X. Tu, Plasma-catalytic removal of formaldehyde over Cu-Ce catalysts in a dielectric barrier discharge reactor, *Appl. Catal. B: Environ.* 170–171 (2015) 293–300.
- [6] S. Hinokuma, N. Yamashita, Y. Katsuhara, H. Kogami, M. Machida, CO oxidation activity of thermally stable Fe-Cu/CeO₂ catalysts prepared by dual-mode arc-plasma process, *Catal. Sci. Technol.* 5 (2015) 3945–3952.
- [7] Y. Li, B.W.L. Jang, Selective hydrogenation of acetylene over Pd/Al₂O₃ catalysts: effect of non-thermal RF plasma preparation methodologies, *Top. Catal.* 60 (2017) 997–1008.
- [8] E. Antolini, Photo-assisted methanol oxidation on Pt-TiO₂ catalysts for direct methanol fuel cells: a short review, *Appl. Catal. B: Environ.* 237 (2018) 491–503.
- [9] L. Pastor-Pérez, V. Belda-Alcázar, C. Marini, M.M. Pastor-Blas, A. Sepúlveda-Escribano, E.V. Ramos-Fernandez, Effect of cold Ar plasma treatment on the catalytic performance of Pt/CeO₂ in water-gas shift reaction (WGS), *Appl. Catal. B: Environ.* 225 (2018) 121–127.
- [10] R.V. Gulyaev, E.M. Slavinskaya, S.A. Novopashin, D.V. Smovzh, A.V. Zaikovskii, D.Y. Osadchii, O.A. Bulavchenko, S.V. Korenev, A.I. Boronin, Highly active PdCeO_x composite catalysts for low-temperature CO oxidation, prepared by plasma-arc synthesis, *Appl. Catal. B: Environ.* 147 (2014) 132–143.
- [11] X. Zhu, S. Liu, Y. Cai, X. Gao, J. Zhou, C. Zheng, X. Tu, Post-plasma catalytic removal of methanol over Mn-Ce catalysts in an atmospheric dielectric barrier discharge, *Appl. Catal. B: Environ.* 183 (2016) 124–132.
- [12] S. Zhao, K. Li, S. Jiang, J. Li, Pd-Co based spinel oxides derived from pd nanoparticles immobilized on layered double hydroxides for toluene combustion, *Appl. Catal. B: Environ.* 181 (2016) 236–248.
- [13] Y. Guo, X. Liao, J. He, W. Ou, D. Ye, Effect of manganese oxide catalyst on the

- dielectric barrier discharge decomposition of toluene, *Catal. Today* 153 (2010) 176–183.
- [14] F. Rahmani, M. Haghghi, P. Estifaei, Synthesis and characterization of Pt/ $\text{Al}_2\text{O}_3\text{-CeO}_2$ nanocatalyst used for toluene abatement from waste gas streams at low temperature: conventional vs. plasma–ultrasound hybrid synthesis methods, *Micropor. Mesopor. Mater.* 185 (2014) 213–223.
- [15] H. Chen, X. Jia, Y. Li, C. Liu, Y. Yang, Controlled surface properties of Au/ZSM5 catalysts and their effects in the selective oxidation of ethanol, *Catal. Today* 256 (2015) 153–160.
- [16] M. Lu, R. Huang, P. Wang, L. Chen, J. Wu, M. Fu, W. Wen, B. Huang, D. Ye, Plasma-catalytic oxidation of toluene on Mn O_x at atmospheric pressure and room temperature, *Plasma Chem. Plasma Process.* 34 (2014) 1141–1156.
- [17] S. Hinokuma, H. Fujii, Y. Katsuhara, K. Ikeue, M. Machida, Effect of thermal ageing on the structure and catalytic activity of Pd/ CeO_2 prepared using arc-plasma process, *Catal. Sci. Technol.* 4 (2014) 2990–2996.
- [18] M.J. Wolf, J. Kullgren, P. Broqvist, K. Hermansson, Fluorine impurities at $\text{CeO}_2(111)$: effects on oxygen vacancy formation, molecular adsorption, and surface re-oxidation, *J. Chem. Phys.* 146 (2017) 044703.
- [19] B. Liu, J. Liu, S. Ma, Z. Zhao, Y. Chen, X.-Q. Gong, W. Song, A. Duan, G. Jiang, Mechanistic study of selective catalytic reduction of NO with NH_3 on W-doped CeO_2 catalysts: unraveling the catalytic cycle and the role of oxygen vacancy, *J. Phys. Chem. C* 120 (2016) 2271–2283.
- [20] T. Andana, M. Piumetti, S. Bensaid, L. Veyre, C. Thieuleux, N. Russo, D. Fino, E.A. Quadrelli, R. Pirone, Ceria-supported small Pt and Pt₃Sn nanoparticles for NO_x-assisted soot oxidation, *Appl. Catal. B: Environ.* 209 (2017) 295–310.
- [21] T. Andana, M. Piumetti, S. Bensaid, L. Veyre, C. Thieuleux, N. Russo, D. Fino, E.A. Quadrelli, R. Pirone, Nanostructured equimolar ceria-praseodymia for NO_x-assisted soot oxidation: insight into Pr dominance over Pt nanoparticles and metal-support interaction, *Appl. Catal. B: Environ.* 226 (2018) 147–161.
- [22] A.M. Gänzler, M. Casapu, F. Maurer, H. Störmer, D. Gerthsen, G. Ferré, P. Vernoux, B. Bornmann, R. Frahm, V. Murzin, M. Nachtegaal, M. Votsmeier, J.-D. Grunwaldt, Tuning the Pt/ CeO_2 interface by in situ variation of the Pt particle size, *ACS Catal.* 8 (2018) 4800–4811.
- [23] C. Chen, F. Chen, L. Zhang, S. Pan, C. Bian, X. Zheng, X. Meng, F. Xiao, Importance of platinum particle size for complete oxidation of toluene over Pt/ZSM-5 catalysts, *Chem. Commun.* 51 (2015) 5936–5938.
- [24] R. Peng, S. Li, X. Sun, Q. Ren, L. Chen, M. Fu, J. Wu, D. Ye, Size effect of Pt nanoparticles on the catalytic oxidation of toluene over Pt/ CeO_2 catalysts, *Appl. Catal. B: Environ.* 220 (2018) 462–470.
- [25] N. Su, X. Hu, J. Zhang, H. Huang, J. Cheng, J. Yu, C. Ge, Plasma-induced synthesis of Pt nanoparticles supported on Ti O_2 nanotubes for enhanced methanol electro-oxidation, *Appl. Surf. Sci.* 399 (2017) 403–410.
- [26] J. Cole, Y. Zhang, T. Liu, C. Liu, R.M. Sankaran, Process scale-up considerations for non-thermal atmospheric-pressure plasma synthesis of nanoparticles by homogeneous nucleation, *J. Phys. D: Appl. Phys.* 50 (2017) 304001.
- [27] Y. Zhang, K. Van Laer, E.C. Neyts, A. Bogaerts, Can plasma be formed in catalyst pores? A modeling investigation, *Appl. Catal. B: Environ.* 185 (2016) 56–67.
- [28] R. Peng, X. Sun, S. Li, L. Chen, M. Fu, J. Wu, D. Ye, Shape effect of Pt/ CeO_2 catalysts on the catalytic oxidation of toluene, *Chem. Eng. J.* 306 (2016) 1234–1246.
- [29] L. Wang, Y. Zhu, J.Q. Wang, F. Liu, J. Huang, X. Meng, J.M. Basset, Y. Han, F.S. Xiao, Two-dimensional gold nanostructures with high activity for selective oxidation of carbon-hydrogen bonds, *Nat. Commun.* 6 (2015) 6957.
- [30] Z. Wang, Y. Zhang, E.C. Neyts, X. Cao, X. Zhang, B.W.L. Jang, C. Liu, Catalyst preparation with plasmas: how does it work? *ACS Catal.* 8 (2018) 2093–2110.
- [31] E.C. Neyts, Plasma-surface interactions in plasma catalysis, *Plasma Chem. Plasma Process.* 36 (2015) 185–212.
- [32] Y. Guo, D. Ye, K. Chen, J. He, Toluene removal by a DBD-type plasma combined with metal oxides catalysts supported by nickel foam, *Catal. Today* 126 (2007) 328–337.
- [33] A.H.A. Beck, A. Szucs, Z. Schay, Z. Zsoldos, I. Dany, L. Guczi, Pd nanoparticles prepared by “controlled colloidal synthesis” in solid/liquid interfacial layer on silica, *Catal. Lett.* 65 (2000) 33–42.
- [34] M. Hatanaka, N. Takahashi, N. Takahashi, T. Tanabe, Y. Nagai, A. Suda, H. Shinjoh, Reversible changes in the Pt oxidation state and nanostructure on a ceria-based supported Pt, *J. Catal.* 266 (2009) 182–190.
- [35] M. Liu, X. Wu, S. Liu, Y. Gao, Z. Chen, Y. Ma, R. Ran, D. Weng, Study of Ag/ CeO_2 catalysts for naphthalene oxidation: balancing the oxygen availability and oxygen regeneration capacity, *Appl. Catal. B: Environ.* 219 (2017) 231–240.
- [36] Q. Ren, S. Mo, R. Peng, Z. Feng, M. Zhang, L. Chen, M. Fu, J. Wu, D. Ye, Controllable synthesis of 3D hierarchical Co₃O₄ nanocatalysts with various morphologies for the catalytic oxidation of toluene, *J. Mater. Chem. A* 6 (2018) 498–509.
- [37] M. Xu, T.S. Li, M. Yang, M. Andersson, I. Fransson, T. Larsson, B. Sundén, Modeling of an anode supported solid oxide fuel cell focusing on thermal stresses, *Int. J. Hydrogen Energy* 41 (2016) 14927–14940.
- [38] M. Vandebossche, D. Hegemann, Recent approaches to reduce aging phenomena in oxygen- and nitrogen-containing plasma polymer films: an overview, *Curr. Opin. Solid State Mater. Sci.* 22 (2018) 26–38.
- [39] L. Artiglia, F. Orlando, K. Roy, R. Kopelent, O. Safonova, M. Nachtegaal, T. Huthwelker, J.A. van Bokhoven, Introducing time resolution to detect Ce(3+) catalytically active sites at the Pt/ CeO_2 interface through ambient pressure X-ray photoelectron spectroscopy, *J. Phys. Chem. Lett.* 8 (2017) 102–108.
- [40] J.M. López, A.L. Gilbank, T. García, B. Solsona, S. Agouram, L. Torrente-Murciano, The prevalence of surface oxygen vacancies over the mobility of bulk oxygen in nanostructured ceria for the total toluene oxidation, *Appl. Catal. B: Environ.* 174–175 (2015) 403–412.
- [41] S. Damyanova, B. Pawelec, R. Palcheva, Y. Karakirova, M.C.C. Sanchez, G. Tyuliev, E. Gaigneaux, J.L.G. Fierro, Structure and surface properties of ceria-modified Ni-based catalysts for hydrogen production, *Appl. Catal. B: Environ.* 225 (2018) 340–353.
- [42] F. Wang, S. He, H. Chen, B. Wang, L. Zheng, M. Wei, D.G. Evans, X. Duan, Active site dependent reaction mechanism over Ru/ CeO_2 catalyst toward CO₂ methanation, *J. Am. Chem. Soc.* 138 (2016) 6298–6305.
- [43] E.M. Slavinskaya, A.I. Stadnichenko, V.V. Muravyov, T.Y. Kardash, E.A. Derevyannikova, V.I. Zaikovskii, O.A. Stonkus, I.N. Lapin, V.A. Svetlichnyi, A.I. Boronin, Transformation of a Pt- CeO_2 mechanical mixture of pulsed-laser-ablated nanoparticles to a highly active catalyst for carbon monoxide oxidation, *ChemCatChem* 10 (2018) 2232–2247.
- [44] S.F. Friedrich Esch, Ling Zhou, Tiziano Montini, Cristina Africh, Paolo Fornasiero, Giovanni Comelli, Renzo Rosei, Electron localization determines defect formation on ceria substrates, *Science* 309 (2005) 749–752.
- [45] S. Agarwal, X. Zhu, E.J.M. Hensen, L. Lefferts, B.L. Mojet, Defect chemistry of ceria nanorods, *J. Phys. Chem. C* 118 (2014) 4131–4142.
- [46] Y.K. Chae, S. Mori, M. Suzuki, Visible-light photocatalytic activity of anatase Ti O_2 treated with argon plasma, *Thin Solid Films* 517 (2009) 4260–4263.
- [47] J. Van Durme, D. Dewulf, C. Leyns, H. Van Langenhove, Combining non-thermal plasma with heterogeneous catalysis in waste gas treatment: a review, *Appl. Catal. B: Environ.* 78 (2008) 324–333.
- [48] Y. Liao, C. He, C. Man, L. Chen, M. Fu, J. Wu, D. Ye, B. Huang, Diameter-dependent catalytic activity of ceria nanorods with various aspect ratios for toluene oxidation, *Chem. Eng. J.* 256 (2014) 439–447.
- [49] L. Nie, D. Mei, H. Xiong, B. Peng, Z. Ren, X.I.P. Hernandez, A. DeLaRiva, M. Wang, M.H. Engelhard, L. Kovarik, A.K. Datye, Y. Wang, Activation of surface lattice oxygen in single-atom Pt/ CeO_2 for low-temperature CO oxidation, *Science* 358 (2017) 1419–1423.
- [50] N. Acerbi, S.C. Tsang, G. Jones, S. Golunski, P. Collier, Rationalization of interactions in precious metal/ceria catalysts using the d-band center model, *Angew. Chem. Int. Ed. Engl.* 52 (2013) 7737–7741.
- [51] Y.T. Lai, T.C. Chen, Y.K. Lan, B.S. Chen, J.H. You, C.M. Yang, N.C. Lai, J.H. Wu, C.S. Chen, Pt-SBA-15 as a highly efficient catalyst for catalytic toluene oxidation, *ACS Catal.* 4 (2014) 3824–3836.
- [52] A. Kulkarni, S. Siahrastami, A. Patel, J.K. Norskov, Understanding catalytic activity trends in the oxygen reduction reaction, *Chem. Rev.* 118 (2018) 2302–2312.
- [53] S. Wei, Y. Zhao, G. Fan, L. Yang, F. Li, Structure-dependent selective hydrogenation of cinnamaldehyde over high-surface-area Ce O_2 –Zr O_2 composites supported Pt nanoparticles, *Chem. Eng. J.* 322 (2017) 234–245.
- [54] D. Mei, X. Zhu, C. Wu, B. Ashford, P.T. Williams, X. Tu, Plasma-photocatalytic conversion of CO₂ at low temperatures: understanding the synergistic effect of plasma-catalysis, *Appl. Catal. B: Environ.* 182 (2016) 525–532.
- [55] F. Wang, C. Li, X. Zhang, M. Wei, D.G. Evans, X. Duan, Catalytic behavior of supported Ru nanoparticles on the {100}, {110}, and {111} facet of Ce O_2 , *J. Catal.* 329 (2015) 177–186.
- [56] A. Trovarelli, Catalytic properties of ceria and Ce O_2 -containing materials, *Catal. Rev.* 38 (1996) 439–520.
- [57] J. Lee, Y. Ryoo, X. Chan, T.J. Kim, D.H. Kim, How Pt interacts with Ce O_2 under the reducing and oxidizing environments at elevated temperature: the origin of improved thermal stability of Pt/Ce O_2 compared to Ce O_2 , *J. Phys. Chem. C* 120 (2016) 25870–25879.
- [58] Y. Wang, G. Song, Z. Xu, F. Rosei, D. Ma, G. Chen, Interfacial reaction-directed synthesis of a ceria nanotube-embedded ultra-small Pt nanoparticle catalyst with high catalytic activity and thermal stability, *J. Mater. Chem. A* 4 (2016) 14148–14154.
- [59] Y. Wu, W. Chung, M. Chang, Modification of Ni/ $\gamma\text{-Al}_2\text{O}_3$ catalyst with plasma for steam reforming of ethanol to generate hydrogen, *Int. J. Hydrogen Energy* 40 (2015) 8071–8080.
- [60] G.M. Mullen, E.J. Evans, I. Sabzevari, B.E. Long, K. Alhazmi, B.D. Chandler, C.B. Mullins, Water influences the activity and selectivity of ceria-supported gold catalysts for oxidative dehydrogenation and esterification of ethanol, *ACS Catal.* 7 (2017) 1216–1226.